Molecular Chain Stretch is a Multiaxial Failure Criterion for Conventional and Highly Crosslinked UHMWPE

J.S. Bergström[1*], C.M. Rimnac[2] , S.M. Kurtz[1,3]

[1]Exponent, Inc., 21 Strathmore Rd, Natick, MA
mailto:jorgen@polymerFEM.com

[2]Musculoskeletal Mechanics and Materials Laboratories,
Departments of Mechanical and Aerospace Engineering and Orthopaedics,
Case Western Reserve University, Cleveland, OH

[2]Implant Research Center, School of Biomedical Engineering, Science
and Health Systems, Drexel University, 3141 Chestnut St., Philadelphia PA

Accepted by *Journal of Orthopaedic Research*, August, 2004

Abstract

The development of accurate theoretical failure, fatigue, and wear models for ultra-high molecular weight polyethylene (UHMWPE) is an important step towards better understanding the micromechanisms of the surface damage that occur in load bearing orthopaedic components and improving the lifetime of joint arthoplasties. Previous attempts to analytically predict the clinically observed damage, wear and fatigue failure modes have met limited success due to the complicated interaction between microstructure deformations and continuum level stresses. In this work, we examined monotonic uniaxial and multiaxial loading to failure of UHMWPE using eight failure criteria (maximum principal stress, Mises stress, Tresca stress, hydrostatic stress, Coulomb stress, maximum principal strain, Mises strain, and chain stretch). The quality of the predictions of the different models was assessed by comparing uniaxial tension and small punch test data at different rates with the failure model predictions. The experimental data was obtained for two conventional (unirradiated and gamma radiation sterilized in nitrogen) and two highly crosslinked (150 kGy, remelted and annealed) UHMWPE materials. Of the different failures models examined, the chain stretch failure model was found to most accurately capture uniaxial and multiaxial failure data for both the conventional and the highly crosslinked UHMWPE materials. In addition, the chain stretch failure criterion can readily be calculated for contemporary UHMWPE materials based on available uniaxial tension data. These results lay the foundation for future developments of damage and wear models capable of predicting multiaxial failure under cyclic loading conditions.

Key Words—constitutive modeling, failure modeling, ultra-high molecular weight polyethylene, damage, multiaxial mechanical behavior.

1. Introduction

Mechanical failure of ultra-high molecular weight polyethylene (UHMWPE) components is one of the major factors controlling the lifetime of total joint arthoplasties. The failures that occur *in vivo* are often introduced by contact damage in the form of wear and fatigue [18] caused by relative sliding motion between different components, primarily due to metal-to-polymer interactions. To increase the long-term performance of total joint arthroplasties, investigators have attempted to understand the micromechanisms underlying surface damage in UHMWPE components [29, 30]. The reasoning for this approach is that a fundamental understanding of the micromechanisms of surface damage will facilitate predictions of performance on the component level, which in turn can enable design and material improvements. Despite these efforts, the micromechanics controlling the evolution of surface damage in UHMWPE components are still not fully understood and the state of the art in modeling the failure events is far from complete.

Modeling the damage and failure of UHMWPE, based on micromechanical events, is a challenging task. On the local scale, the material consists of intermixed amorphous and semicrystalline domains. The material behavior is further complicated by the evolving micromechanical state due to applied external loading. Failure of UHMWPE on the microscale is driven by molecular chain scission [12, 17]. The progressive failure events are promoted by the magnified stress and strain state in the neighborhood of already broken molecular chains, resulting in damage localization that is manifested by growth and coalescence of microvoids (also referred to as cavitation) [25, 31].

In general, failure of any polymeric component can be defined as the inability to perform an intended function. Examples of potential failure modes are: excessive plastic deformation, static fracture, fatigue fracture, and wear. This paper focuses on static fracture, which is here defined as loss of material continuity through the formation of new surfaces within the UHMWPE component. This failure mode is the most fundamental, and any failure model of common clinical failure modes, such as fatigue or wear, will need to also address failure under monotonic loading conditions

There are two general classes of failure models for polymers: isostate models and evolving state models. An isostate failure model is a failure model in which the material state is assumed not to change during the applied deformation. The most general isostate failure model is given by

$$f(\mathbf{T},\mathbf{E}) > f_{crit}, \tag{1}$$

where **T** is the current stress state (expressed, for example, in terms of the Cauchy stress tensor), **E** is the current strain state (expressed, for example, in terms of the logarithmic strain tensor), $f(\cdot)$ is a pre-specified failure model, and f_{crit} is a material parameter specifying the critical value of the failure condition. There are two main classes of evolving state models: state variable and history-based models. A general failure condition in state variable form can be written:

$$f\left(\xi_i,\mathbf{T},\mathbf{E}\right) > f_{crit}\ , \tag{2}$$

where ξ_i ($i \in [1, N]$) is a set of state variables specifying the current state. The state variables are assumed to evolve with the deformation according to the rate-equation: $\dot{\xi}_i = g\left(\xi_i,\mathbf{T},\mathbf{E}\right)$, where $g(\cdot)$ is a pre-specified evolution equation.

An evolving state model in history-based form can be written

$$\int_{-\infty}^{t} f\left(\mathbf{T}(t'),\mathbf{E}(t')\right) dt' > f_{crit}\ , \tag{3}$$

where Equation (3) symbolizes that the failure not only depends on the current values of stress and strain, but also on their complete time histories. One interpretation of the history-based integral model can be obtained by defining the integral on the left-hand side of Equation (3) as the damage *D(t)*. The rate of change of damage is then given by $\dot{D}(t) = f(\mathbf{T}, \mathbf{E})$, and the history integral representation can consequently be seen as a special case of the state variable-based evolving state failure model.

The goal of this study was to examine different approaches for predicting static fracture, and then in a later study use this necessary information to address fatigue and wear failures. In this work, we have used monotonic uniaxial and small punch (equibiaxial) tests to failure to examine the relative capabilities of different failure models to predict fracture for two conventional (unirradiated and gamma radiation sterilized in nitrogen) and two highly crosslinked (150 kGy, remelted and annealed) UHMWPE materials. Currently, conventional UHMWPE is the dominant material for hip and knee total joint replacement implants. However, highly crosslinked UHMWPE materials are gaining in use, particularly for hip replacement components, due to improved wear resistance [19].

2. Materials and Methods

There are a number of different types of models that can potentially be used to predict failure of UHMWPE, including: stress-based models; strain-based models; energy-based models; linear elastic fracture mechanics (LEFM) models; and damage models [6]. The first four types of models are constant state models, whereas the damage models are evolving state models. It is unlikely that an energy-based model will be predictive since large strain energy can be stored in hydrostatic compression but the material will not fracture in this mode. LEFM models are a specific case of a stress-based constant state model. Thus, in this study, we examined the following eight isostate failure models: (1) maximum principal stress; (2) Mises stress; (3) Tresca stress; (4) hydrostatic stress; (5) Coulomb stress; (6) maximum principal strain; (7) Mises strain; and (8) chain stretch. Most of these models are well known and are discussed in detail in most introductory solid mechanics textbooks

[20]. For completeness, three of the lesser known models (the Coulomb model, the Mises strain model, and the chain stretch model) are discussed herein in more detail.

The Coulomb stress is defined as

$$\sigma_{Coulomb} = (\sigma_1 - \sigma_3) + \mu(\sigma_1 + \sigma_3) \tag{4}$$

where σ_1 is the largest principal stress, σ_3 is the smallest principal stress, and μ=0.10 is taken as the friction coefficient. The Mises strain is defined analogously to the traditional Mises stress, i.e.

$$\varepsilon_{Mises} = \sqrt{\frac{1}{2}\left[(\varepsilon_1 - \varepsilon_2)^2 + (\varepsilon_2 - \varepsilon_3)^2 + (\varepsilon_3 - \varepsilon_1)^2\right]}, \tag{5}$$

where ε_i are the principal strains.

The chain stretch failure condition is motivated by our recently developed physically-inspired constitutive model for UHWMPE, the Hybrid model (HM) [9, 10]. The HM is based, in part, on some of the constitutive modeling work by Boyce et al. [2, 3, 16] who have successfully modeled, glassy amorphous polymers, semicrystalline polymers, and rubbers. However, these theories did not adequately describe UHMWPE; thus, the HM was developed and validated specifically for semicrystalline UHMWPE. One of the key features of the HM is the concept of molecular chain stretch [7]. In the chain stretch failure model, an estimation of the average molecular chain stretch is given by the expression

$$\lambda_{chain} = \sqrt{\frac{1}{3}\left[e^{2\varepsilon_1} + e^{2\varepsilon_2} + e^{2\varepsilon_3}\right]}, \tag{6}$$

where, as before, ε_1, ε_2, and ε_3 are the principal strains. This representation enables a mapping from the applied deformation state to the local molecular stretch state, and has been examined using molecular dynamics and Monte Carlo simulations [8]. In the chain stretch model, failure is assumed to occur when the average molecular chain stretch reaches a critical level.

To evaluate the quality of the predictions of the different failure models, it is necessary to use appropriate experimental test methods and well-characterized materials. In this study, we examined four different types of UHMWPE obtained from ram-extruded rods of GUR 1050 that were subjected to different radiation and heat treatments. The four materials [20] were: (1) as-received unirradiated; (2) gamma radiation sterilized in Nitrogen with 30 kGy; (3) gamma radiation treated with 100 kGy, giving a highly crosslinked microstructure, and subsequently annealed at 110°C for 2 hours; and (4) gamma radiation treated with 100 kGy, giving a highly crosslinked microstructure, and subsequently remelted at 150°C. The microstructures of the materials studied in this work have been extensively examined elsewhere [20]; e.g., the degree of crystallinity of the three materials was determined to be 0.50 for the unirradiated, 0.51 for the sterilized material (30 kGy γ-N_2), 0.61 for the crosslinked material heat treated at 110°C, and 0.46 for the crosslinked material heat treated at 150°C. The four materials were tested in uniaxial large strain monotonic tension to failure and in small punch testing to failure.

2.1 Uniaxial Tension to Failure Experiments

The stress-strain behavior from the uniaxial tension to failure tests has been reported previously [16] for the four materials examined in this study. Uniaxial tension behavior of other types of conventional and crosslinked UHMWPE have been reported in other studies [1, 13, 15, 21-23, 27]. Briefly, the uniaxial tension to failure experiments used specimens that were prepared and tested according to ASTM D638 [4]. The testing was performed using a 4204 Instron electromechanical load frame, equipped with a 5 kN load cell. The specimens were tested under displacement control at crosshead displacement rates of 30, 75, and 150 mm/min, approximately corresponding to initial true strain rates of 0.01/s, 0.02/s, and 0.05/s. A non-contacting video extensometer was used to measure axial strain [20]. Five specimens were tested for each experimental condition, corresponding to a total of 60 specimens (5 specimens per material × 4 materials × 3 rates).

2.2 Small Punch Testing to Failure

The load-displacement behavior from the small punch failure tests has been reported previously [18]. Briefly, the small punch testing was performed on disc shaped specimens measuring 6.4 mm in diameter and 0.5 mm in thickness. The specimens were tested using an MTS Model 859 testing machine by indentation with a custom-built, hemispherical head punch at three different punch displacement rates (0.5 mm/min, 1.0 mm/min, and 5.0 mm/min). The tests were performed at room temperature (20°C ± 2°C), according to ASTM F2183-02 [5]. Five specimens were tested for each experimental condition, corresponding to a total of 60 specimens (5 specimens per material × 4 materials × 3 rates).

The experimental data obtained from the small punch tests is in terms of force and displacement of the punch head. This data can be converted to stress and strain by simulating the small punch tests using the finite element (FE) method. To perform these FE simulations an axisymmetric representation of the experimental setup was created (Figure 1). In this FE representation, the test specimen was modeled with 360 quadratic axisymmetric elements, and the punch and fixture were assumed to be rigid. The FE simulations were performed using the commercial finite element package ABAQUS (HKS Inc., RI).

To accurately determine the stress and strain distributions in the test specimens, it is necessary to have an accurate constitutive model capable of predicting the material behavior in large-strain multiaxial deformation states. In this work we used the HM [9-11]. The HM has been calibrated and validated for the four UHMWPE materials that are used in this study. The material parameters that are used in the simulations of the four materials and a brief summary of the HM are presented in Appendix A.

To enable failure predictions of the small punch testing, a total of 12 FE simulations were performed (4 materials × 3 rates). In these simulations the punch was displaced to the maximum displacement value that was experimentally observed in the five repeated experiments on that specific material and applied displacement rate. The maximum stress and strain values at the experimentally observed failure states for each of the five repeated tests were then extracted from the FE simulations by finding the location having the maximum stress and strain and extracting the stress and strain tensors at that location.

2.3 Failure Modeling

The failure parameters for each material (e.g. the Mises stress at failure) were obtained from the average of the experimentally observed values from all uniaxial and small punch tests. The quality of the different failure models was evaluated by comparing the predicted failure values for the two loading modes at each of the three displacement rates. The quality of the predictions was quantified with the coefficient of determination [9], r^2, between the experimental failure values and the predicted failure condition for each material. The predicted failure condition was assumed to be independent of loading rate.

The predictive capability of each model was also graphically represented using "box and whiskers" plots. In these plots, the center 50% percentiles of the data are represented using a box. The median is represented with a horizontal line inside the box. The 90% and 10% percentiles are represented with vertical bars extending outside the box, and any outlying data points outside the 90% and 10% percentiles are individually represented by small circles. Thus, the relative ability of the eight failure models to predict failure was examined by comparing the predicted failure value in the different experimental tests for each of the materials, and by assessing if the predicted failure values for each material tended to have a constant value at the observed failure instances.

To evaluate the different failure models, it is necessary to know the stress and strain distributions in the test specimens as a function of the applied deformation. For the uniaxial tension tests, the stress and strain distributions are directly obtained from the experimentally determined force-displacement curves. For the small punch tests, we obtained the stress-strain response by simulating the experimental tests using the finite element (FE) method. The FE simulations were based on the Hybrid Model (HM) [7-9] to represent the material behavior.

3. Results

The capabilities of the HM to predict the behavior of the UHMWPE is shown in Figures 2(a) and (b). These figures present a direct comparison between experimental data for the highly crosslinked UHMWPE material that was annealed at 110°C and predictions from the HM. Figure 3(a) shows the response in uniaxial tension at three different deformation rates. Figure 3(b) shows the force-displacement response from five repeated small punch test performed at a punch displacement rate of 0.5 mm/min. The failure points, indicated with the symbol □ in the figures, occurred at different applied deformations, but the experimental force-displacement responses are all very repeatable. As discussed by Bergström et al. [9-11] and illustrated in Figure 3, the HM is an accurate constitutive model for predicting the behavior of the different types of UHMWPE investigated in this work.. It can be seen that the failure strengths of the two highly crosslinked materials in uniaxial tension are lower than for the two conventional materials, but that the highly crosslinked materials fail at higher forces than the conventional materials when tested in small punch (equibiaxial) loading. This behavior is caused by different evolutions of the microstructural deformations when tested in uniaxial and multiaxial tests [11].

The results from applying the eight failure models to the experimental data for the four UHMWPE materials are summarized in Table 1. The results from applying the different failure models to the experimental data are also graphically presented in box and whisker plots in Figures 4(a) to 4(h). The results for the maximum principal stress, Mises stress, and Tresca stress models show that these three failure models behave similarly (Table 1) and have almost identical failure conditions (Figures 4(a), (b), (c), respectively). They also show good predictive agreement between the uniaxial and the multiaxial failure data for all materials except the highly crosslinked material that was heat treated at 150°C. For this latter material, the effective stress value is significantly higher in the small punch tests than in the uniaxial tests. There is also a large scatter in the effective stress values at failure for these three failure models (Figures 4(a), (b), (c)). The variation in stress at failure for the unirradiated UHMWPE tested in uniaxial tension to failure, for example, varies between 150 and 320 MPa.

The predicted hydrostatic stress in the specimen at the time of failure is significantly higher in the small punch tests than in the uniaxial tests (Figure 4(d)). Hence, the hydrostatic stress model is not useful as a general failure predictor of UHMWPE. The Coulomb model is both qualitatively and quantitatively similar to the Mises, Tresca, and maximum principal stress models (Figure 4(e)). For all materials, the maximum principal strain at failure is larger in uniaxial tension than in the small punch experiments (Figure 4(f)). This is reasonable since the strain state at the tip of the small punch specimen at the time of failure is close to biaxial, and typically lower than in uniaxial tension. The experimentally determined Mises strain at failure is substantially different in uniaxial tension and small punch loading, clearly indicating that the Mises strain is not an accurate general failure predictor (Figure 4(g)).

In contrast to the other failure models, using the chain stretch failure model, there is very good agreement between the predicted failure in uniaxial tension and in small punch loading, for all four materials (Figure 4(h)). Further, the variability in the critical chain stretch between different tests performed at different loading rates is small, relative to the other failure models (Figure 4(h)). The value of the limiting chain stretch (λ_A^{lock}), a material parameter in the HM that specifies how much the molecules can stretch before becoming fully extended is also shown in Figure 4(h). It appears that failure occurs when the molecular chain stretch reaches a certain fraction (60%-80%) of the fully extended chain stretch (Table 2).

A direct comparison between the quantitative performances of the different failure models, by examination of the r^2-values between all experimental failure data and the critical failure values for the four materials demonstrates that the predictions from the chain stretch model have a much lower variability between different tests and better overall agreement with both uniaxial and multiaxial experimental failure data than the other failure models (Figure 5). The r^2-value for the chain stretch model is about 0.85. That is, the chain stretch model describes 85% of the variability in the failure data for a broad range of UHMWPE materials, loading conditions, and loading rates. Of the other models, the Mises stress, the maximum principal stress, Tresca stress, Coulomb stress and maximum principal strain are about equal, each having a r^2-value of about 0.55. The hydrostatic stress and the Mises strain models are clearly the poorest performers, both having r^2-values less than 0.2.

4. Discussion

The experimental results and model predictions presented in this report indicate that uniaxial and multiaxial failure of conventional and highly crosslinked UHMWPE under monotonic loading can be accurately predicted using the chain stretch model. The chain stretch model is interesting not only because it provides the most accurate predictions of the models tested, but also due to its relationship to the stretching of the macromolecules in the material and with the maximum chain locking stretch parameter in the Hybrid model. The correlation between the experimental chain stretch at failure and the chain locking parameter suggests that if the HM is calibrated for a given UHMWPE material, then a good multiaxial failure condition can likely be obtained by taking the chain stretch at failure to be about 60% to 80% of the chain locking stretch parameter.

In practical terms, the chain stretch at failure for UHMWPE materials can be directly measured during standard uniaxial tensile tests. The chain stretch at failure is related to the uniaxial strain at failure (ε) by the following equation:

$$\lambda_{chain} = \sqrt{\frac{1}{3}\left[e^{2\varepsilon} + 2e^{-\varepsilon}\right]} \tag{7}$$

Uniaxial tensile tests are a standard method for characterizing the mechanical properties for conventional and highly crosslinked UHMWPE (e.g., ASTM F-648). Consequently, the chain stretch failure criterion outlined in the present study can readily be calculated for contemporary UHMWPE materials based on available experimental data.

Some of the other failure models, e.g. the maximum principal stress and the Mises stress models, provide reasonable failure predictions of the uniaxial and small punch data. The scatter in the experimental failure criteria from these models, however, makes them less useful as a failure predictor under multiaxial loading conditions.

The results from this study also suggest that the failure conditions for conventional and highly crosslinked UHMWPE depend on radiation dose and heat treatment (Table 1). One particularly interesting trend is observed when comparing the experimental failure data with the failure predictions of the different models. The failure of the unirradiated and the sterilized materials are both nicely captured by either a stress-based model (maximum principal stress, Mises stress, or Tresca stress) or by the chain stretch model. However, for the two highly crosslinked materials (particularly the remelted material 100 kGy, 150°C), the stress-based failure models tend to underestimate the strength in the small punch experiments and overestimate the strength in the uniaxial experiments. The only model capable of accurately predicting the behavior of these materials is the chain stretch model.

It is also interesting to consider the molecular weight between crosslinks and how it may relate to the maximum chain stretch. The concept of a molecular weight between crosslinks is derived from Flory's [14] statistical theories for a swollen crosslinked polymer network in equilibrium with a good solvent. In contrast, the maximum chain stretch in our failure theory reflects the amount of local deformation that can be accommodated by UHMWPE, regardless of whether or not it is crosslinked. For virgin UHMWPE, the molecular weight between crosslinks is theoretically infinite, thus, there is no relationship between molecular weight between crosslinks and maximum chain stretch for the unirradiated UHMWPE examined in this study. With respect to the materials considered in our study, the molecular weight between crosslinks decreases from infinity (for unirradiated UHMWPE) to an estimated value of 6,000 g/mol at a dose of 100 kGy [28]. For this reason, we do not judge the molecular weight between crosslinks to be an attractive state variable for predicting the failure behavior of conventional and highly crosslinked UHMWPE.

It is known that the material response of UHMWPE is rate-dependent [9]. By performing an analysis of variance (ANOVA) on the experimental data obtained at different loading rates it is possible to examine if the failure quantities are rate-dependent. A direct analysis of the experimental data shows that the only rate-effects that are statistically significant ($p < 0.05$) are: (1) the punch force at failure increases with increasing punch rate; (2) the punch displacement at failure decreases with increasing punch rate for the unirradiated material. The other failure quantities, e.g. the stress and strain response in uniaxial tension, showed no statistically significant rate-dependence [20]. Overall, these findings support our assumption that the failure criteria for UHMWPE is effectively rate independent.

The high stress and strain values at failure that are reported in Table 1 are indicative of the intrinsic strength of the material and can be used to predict material failure on the microscale at the tip of microcracks or the local damage during wear. A complicating factor when studying failure of polymeric components is that failure of seemingly identical components typically occurs at different load levels. The apparent distribution in failure strengths is caused by variations in the internal state of the material in different components. The differences can, for example, be due to localized differences in molecular weight, molecular weight distribution, crosslinking density, degree of crystallinity, morphology, or defect population. The failure on a macroscopic scale therefore often appears stochastic. The results presented here for monotonic loading lay the foundation for the future development of more advanced stochastic damage models that can accurately predict failure under multiaxial, cyclic loading conditions.

5. Acknowledgement

This work was supported by NIH Grant 1 R01 AR 47192. Thanks also to M. Villarraga and L. Ciccarelli for assistance with the small punch tests.

Appendix A.

This appendix briefly summarizes the governing equations of the Hybrid Model (HM). For a more in depth discussion, see the recent publications by Bergström et al. [9, 10].

The kinematic framework used in the HM is based on a conceptual homogenization of the semi-crystalline and amorphous domains [2, 3, 16],and a decomposition of the deformation gradient into elastic and viscoplastic components: $\mathbf{F} = \mathbf{F}^e\,\mathbf{F}^p$. The Cauchy stress acting on the system can be obtained from the linear elastic relationship:

$$\mathbf{T} = \frac{1}{J^e}\left(2\mu^e\mathbf{E}^e + \lambda\,\mathrm{tr}\left[\mathbf{E}^e\right]\mathbf{1}\right), \tag{a1}$$

where $\mathbf{E}^e = \ln[\mathbf{V}^e]$ is the logarithmic true strain, $J^e = \det[\mathbf{F}^e]$, and μ^e, λ^e are Lamé's constants. For convenience, the Lamé constants can be replaced by the equivalent Young's modulus (E) and Poisson's ratio (ν):$\mu_e = E_e / (2(1+\nu_e))$ and $\lambda_e = E_e\nu_e / ((1+\nu_e)(1-2\nu_e))$.

The details of the stress expressions are presented in Equations (a2) – (a4)

$$\mathbf{T}_A = \frac{1}{1+q_A}\left[\mathbf{T}_{8chain}\left(\mathbf{F}^p;\mu_A,\lambda_A^{lock},\kappa_A\right)+q_A\mathbf{T}_{I_2}\left(\mathbf{F}^p;\mu_A\right)\right], \tag{a2}$$

$$\mathbf{T}_{8chain} = \frac{\mu^p}{\overline{\lambda^p}}\cdot\frac{L^{-1}\left(\overline{\lambda^p}/\lambda^p_{lock}\right)}{L^{-1}\left(1/\lambda^p_{lock}\right)}\mathrm{dev}\left[\mathbf{B}^p\right], \tag{a3}$$

$$\mathbf{T}_{I_2} = \mu_A\left[I_1^{p*}\mathbf{B}^{p*} - \frac{2I_2^{p*}}{3}\mathbf{1} - \left(\mathbf{B}^{p*}\right)^2\right]. \tag{a4}$$

where $\mathbf{T}_A$ is a tensor-valued function of the viscoplastic deformation gradient $\mathbf{F}^p$ and the material parameters $\{\mu_A, \lambda_A^{lock}, \kappa_A, q_A\}$, where μ_A is the shear modulus, λ_A^{lock} is the locking stretch, κ_A is the bulk modulus, and q_A is a material parameter specifying the relative magnitudes of $\mathbf{T}_{8chain}$ and $\mathbf{T}_{I2}$, and $\mathbf{B}^{p*}$ is the left Cauchy-Green deformation tensor,

The stress driving the viscoplastic flow of the backstress network is obtained from the same hyperelastic representation that was used to calculate the backstress: $\mathbf{T}_B = s_B \cdot \mathbf{T}_A\left(\mathbf{F}_B^e\right)$,

where s_B is a dimensionless material parameter specifying the relative stiffness of the backstress network. The parameter s_B evolves with imposed plastic deformation to capture the distributed yielding: $\dot{s}_B = p_B \cdot \left(s_B - s_{Bf}\right)\cdot\dot{\gamma}_C^v$, where p_B is a material parameter specifying the transition rate of the distributed yielding event, s_{Bf} is the final value of s_B reached at fully developed plastic flow, and $\dot{\gamma}_B^v$ is the rate of viscoplastic flow of the time-dependent part of network B:

$$\dot{\gamma}_B^v = \dot{\gamma}_0 \left(\frac{\tau_B}{\tau_B^{base}} \right)^{m_B}, \tag{a5}$$

where $\tau_B = \left\| \text{dev}\left[\mathbf{T}_B\right] \right\|_F$, τ_B^{base} and m_B are material parameters, and $\dot{\gamma}_0$ is a constant coefficient with a value of 1/s. The velocity gradient of the viscoelastic flow of the backstress network is given by

$$\mathbf{L}_B^v = \dot{\gamma}_B^v \mathbf{F}_B^{e-1} \frac{\text{dev}\left[\mathbf{T}_B\right]}{\tau_B} \mathbf{F}_B^e . \tag{a6}$$

The yielding and plastic flow of the material is captured using:

$$\mathbf{L}^p = \dot{\gamma}_C \left[\mathbf{R}^{eT} \frac{\text{dev}[\mathbf{T}_C]}{\tau_C} \mathbf{R}^e \right], \tag{a7}$$

where $\mathbf{L}^p = \dot{\mathbf{F}}^p \mathbf{F}^{p-1}$, $\mathbf{T}_C = \mathbf{T} - [\mathbf{F}^e (\mathbf{T}_A + \mathbf{T}_B) \mathbf{F}^{eT}] / J^e$ is the stress acting on the relaxed configuration convected to the current configuration, $\tau_C = \left\| \text{dev}[\mathbf{T}_C] \right\|_F$ is the effective shear stress (calculated using the Frobenius norm) driving the viscoplastic flow, $\dot{\gamma}_C = \dot{\gamma}_0 \cdot (\tau_C / \tau_C^{base})^{m_C}$ is the magnitude of the viscoplastic flow, τ_C^{base} and m_C are material parameters, and $\dot{\gamma}_0$ a constant coefficient with a value of 1/s.

In total, the augmented HM contains 13 material parameters: 2 small strain elastic constants (E_e, ν_e); 4 hyperelastic constants for the back stress network (μ_A, λ_A^{lock}, κ_A, q_A); 5 flow constants of the backstress network (s_{Bi}, s_{Bf}, p_B, τ_B^{base}, m_B); and 2 yield and viscoplastic flow parameters (τ_C^{base}, m_C). Of these 13 material parameters, four (elastic modulus (E); yield strength (τ_B^{base}); the effective stiffness after yield (μ_A); and the limiting chain stretch (λ_A^{lock}), which controls the large strain behavior) have been shown to vary between UHMWPE formulations, while the remaining nine are constant. The material constants used in the analysis are listed in Table 3. The HM as presented here has, to date, been validated for UHMWPE formulations within the crystallinity range of 46% to 61% and for both uncrosslinked and crosslinked (100 kGy γ-N_2) UHMWPE.

References

[1] Abt NA, Schneider W. Influence of irradiation on the properties of UHMWPE. In Highly Crosslinked and Thermally Treated Ultra-High Molecular Weight Polyethylene For Joint Replacements; Edited by Kurtz, S. M.; Gsell, R.; and Martell, J.; 2003, West Conshohoken, American Society for Testing and Materials.

[2] Arruda EM, Boyce MC. Evolution of Plastic Anisotropy in Amorphous Polymers during Finite Straining. Int. J. Plast. 1993;9: 697-720.

[3] Arruda EM, Boyce MC. Effects of strain rate, temperature and thermomechanical coupling on the finite strain deformation of glassy polymers. Mech. Mater. 1995;19: 193-212.

[4] ASTM D 638-98. Standard Test Method for Tensile Properties of Plastics. In. West Conshohocken, PA: American Society for Testing and Materials, 1998.

[5] ASTM F 2183-02. Standard test method for small punch testing of ultra-high molecular weight polyethylene used in surgical implants. In. West Conshohocken, PA: American Society for Testing and Materials, 2002.

[6] Argon AS, Hannosh JG. Initiation of crazes in Polystyrene. Philos. Mag. 1977;36: 1195-216.

[7] Arruda EM, Boyce MC. A Three-Dimensional Constitutive Model for the Large Stretch Behavior of Rubber Elastic Materials. J. Mech. Phys. Solids 1993;41: 389-412.

[8] Bergström JS, Boyce MC. Deformation of Elastomeric Networks: Relation between Molecular Level Deformation and Classical Statistical Mechanics Models of Rubber Elasticity. Macromolecules 2001;34: 614-26.

[9] Bergström JS, Kurtz SM, Rimnac CM, Edidin AA. Constitutive modeling of ultra-high molecular weight polyethylene under large-deformation and cyclic loading conditions. Biomaterials 2002;23: 2329-43.

[10] Bergström JS, Rimnac CM, Kurtz SM. An Augmented Hybrid Constitutive Model for Simulation of Unloading and Cyclic Loading Behavior of Conventional and Highly Crosslinked UHMWPE. Biomaterials 2004;25 2171-78.

[11] Bergström JS, Rimnac CM, Kurtz SM. Prediction of multiaxial behavior for conventional and highly crosslinked UHMWPE using a hybrid constitutive model. Biomaterials 2003;24: 1365-80.

[12] Browstow W, Corneliussen R. Failure of Plastics. Hanser Publishers, Munich-Vienna-New York, 1986.

[13] Collier JP, Currier BH, Kennedy FE, Currier JH, Timmins GS, Jackson SK, Brewer RL. Comparison of cross-linked polyethylene materials for orthopaedic applications. Clin Orthop. 2003;414: 289-304.

[14] Flory P.J. Principles of Polymer Chemistry, Cornell University Press, 1953.

[15] Greer K, King R, Chan FW. Effects of raw material, irradiation dose, and irradiation source on crosslinking of UHMWPE. In Highly Crosslinked and Thermally Treated Ultra-High Molecular Weight Polyethylene For Joint Replacements; Edited by Kurtz, S. M.; Gsell, R.; and Martell, J.; 2003, West Conshohoken, American Society for Testing and Materials.

[16] Hasan OA, Boyce MC. A Constitutive Model for the Nonlinear Viscoplastic Behavior of Glassy Polymers. Polym. Eng. Sci. 1995;35: 331-344.

[17] Kausch H. Polymer Fracture. Springer-Verlag New York, 1987.

[18] Kurtz SM, Muhlstein C, Edidin AA. Surface morphology and wear mechanisms of four clinically relevant biomaterials after hip simulator testing. J Biomed Mater Res 2000;52: 447-59.

[19] Kurtz SM, Pruitt LA, Jewett CW, Foulds JR, Edidin AA. Radiation and chemical crosslinking promote strain hardening behavior and molecular alignment in ultra high molecular weight polyethylene during multi-axial loading conditions. Biomaterials 1999;20: 1449-62.

[20] Kurtz SM, Villarraga ML, Herr MP, Bergström JS, Rimnac CM, Edidin AA. Thermomechanical behavior of virgin and highly crosslinked ultra-high molecular weight polyethylene used in total joint replacements. Biomaterials 2002;23: 3681-97.

[21] Kurtz SM. Ultra-High Molecular Weight Polyethylene Handbook. 2004; New York, Elsevier Science.

[22] Kurtz SM, Manley M, Wang A, Taylor S, Dumbleton JH. Comparison of the properties of annealed crosslinked (Crossfire) and conventional polyethylene as hip bearing materials. Bull Hosp Jt Dis. 2002-2003;6: 17-27.

[23] Lewis G. Properties of crosslinked ultra-high-molecular-weight polyethylene. Biomaterials. 2001;22: 371-401.

[24] Lubliner J. Plasticity Theory. Macmillan Publishing Company, 1990.

[25] McClintock FA, Argon AS. Mechanical Behavior of Materials. Addison-Wesley Publishing Company, 1965.

[26] McKellop H, Shen FW, Lu B, Campbell P, Salovey R. Development of an extremely wear-resistant ultra high molecular weight polyethylene for total hip replacements. J Orthop Res. 1999;17: 157-67.

[27] Muratoglu OK, Bragdon CR, O'Connor DO, Jasty M, Harris WH. A novel method of cross-linking ultra-high-molecular-weight polyethylene to improve wear, reduce oxidation, and retain mechanical properties. Recipient of the 1999 HAP Paul Award. J Arthroplasty. 2001;16: 149-60.

[28] Spiegelberg S, Kurtz S, Muratoglu O, Greer K, Costa L, Wallace S, Cooper C. Interlaboratory reproducibility of swell ratio measurements for crosslinked UHMWPE. 48th Annual Meeting of the Orthopaedic Research Society, Dallas, TX, 2002.

[29] Sutula LC, Collier JP, Saum KA, Currier BH, Currier JH, Sanford WM, Mayor MB, Wooding RE, Sperling DK, Williams IR, et al. Impact of gamma sterilization on clinical performance of polyethylene in the hip. Clin Orthop 1995;319: 28-40.

[30] White SE, Paxson RD, Tanner MG, Whiteside LA. Effects of sterilization on wear in total knee arthroplasty. Clin Orthop 1996;331: 164-71.

[31] Williams JG. Fracture Mechanics of Polymers. Ellis Horwood Limited, 1987.

List of Figures

Figure 1. Finite element mesh used in the small punch simulations. In the testing, the spherical punch head indented the disc-shaped specimen that was held in place in the fixture by frictional forces. The figure shows the deformed mesh at a punch displacement of 2.0 mm. 23

Figure 2. (a) Uniaxial tension to failure data, (b) small punch loading to failure. The experimental tests were performed on UHMWPE prepared by four different thermal and radiation treatments. 24

Figure 3. Comparison between the experimental data and Hybrid Model predictions: (a) uniaxial tension to failure, (b) small punch testing to failure. The experiments were performed on highly crosslinked UHMWPE annealed at 110°C. The failure points are indicated by the symbol □. 25

Figure 4. Predicted failure conditions in uniaxial tension and small punch loading of the four different types of UHMWPE examined: (a) maximum principal stress; (b) Mises stress; (c) Tresca stress; (d) hydrostatic stress; (e) Coulomb stress; (f) max principal strain; (g) Mises strain; (h) chain stretch. 30

Figure 5. Average r^2-value for all four materials for the different failure models. 31

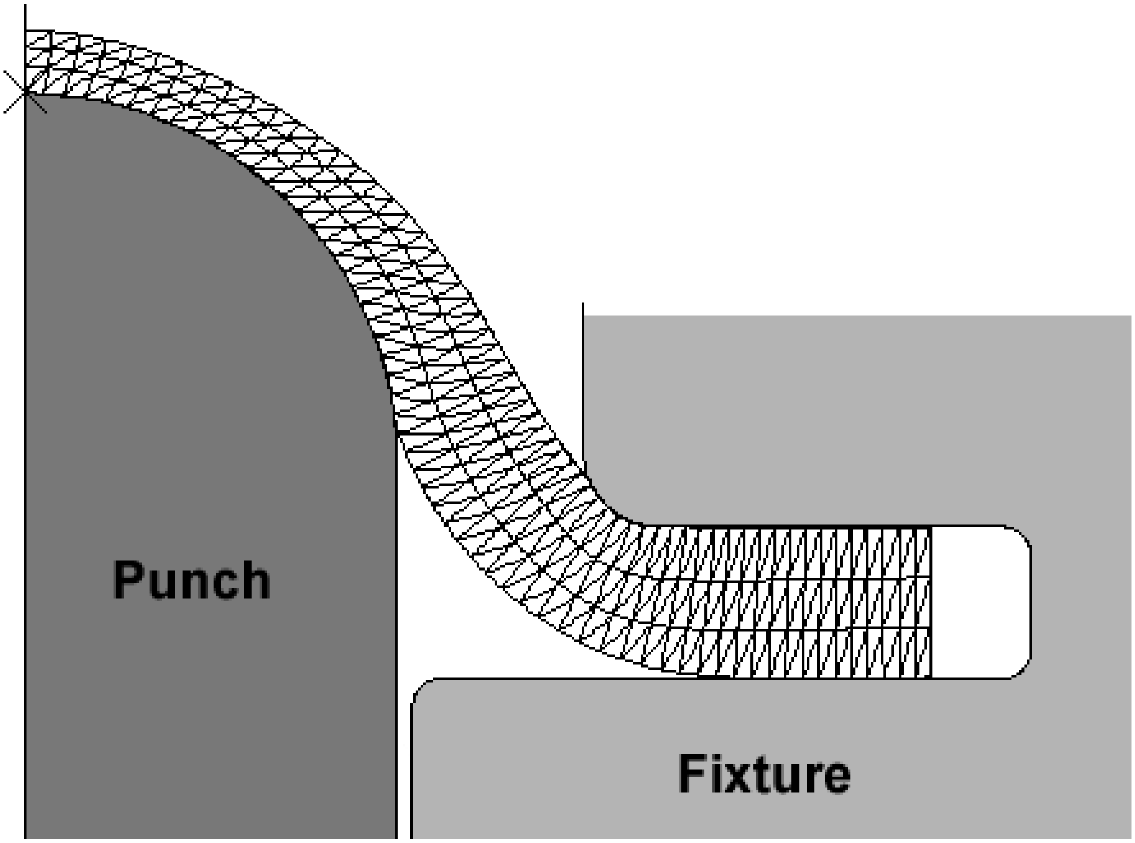

Figure 1. Finite element mesh used in the small punch simulations. In the testing, the spherical punch head indented the disc-shaped specimen that was held in place in the fixture by frictional forces. The figure shows the deformed mesh at a punch displacement of 2.0 mm.

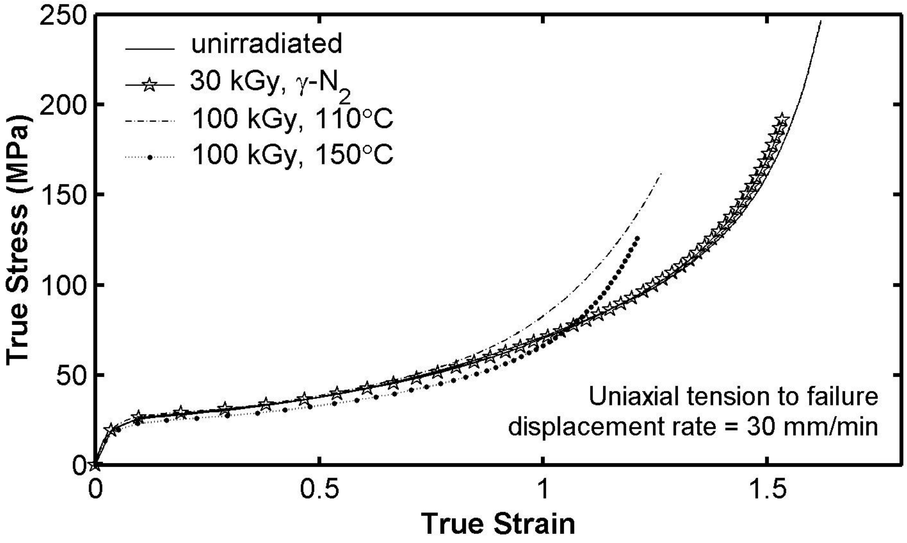

(a)

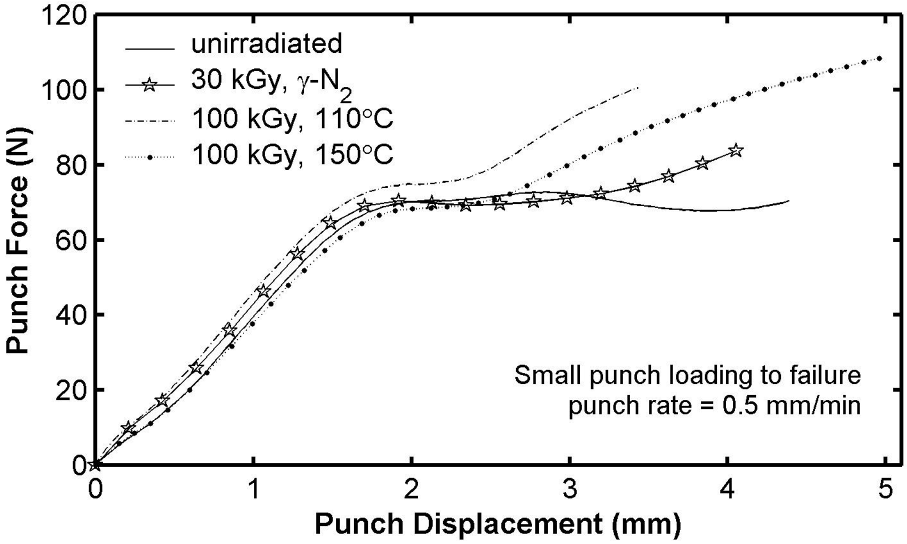

(b)

Figure 2. (a) Uniaxial tension to failure data, (b) small punch loading to failure. The experimental tests were performed on UHMWPE prepared by four different thermal and radiation treatments.

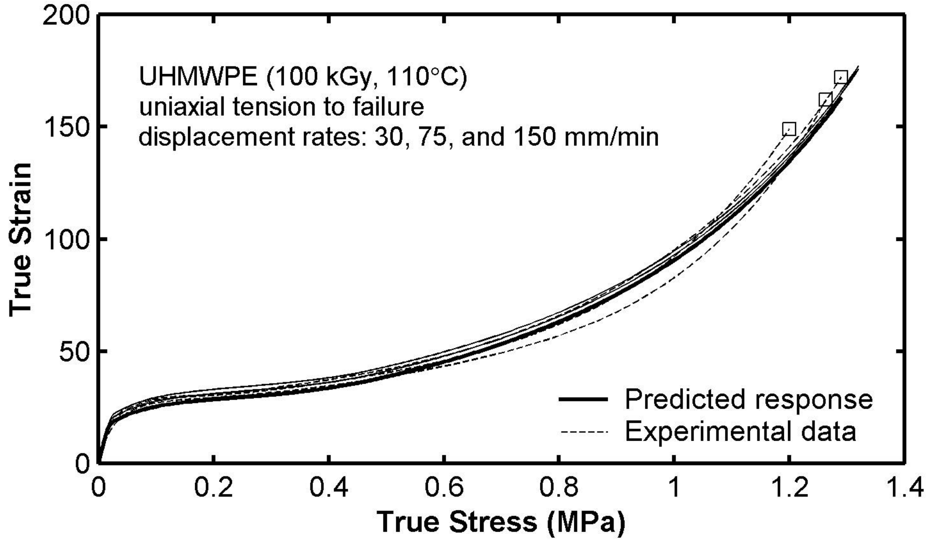

(a)

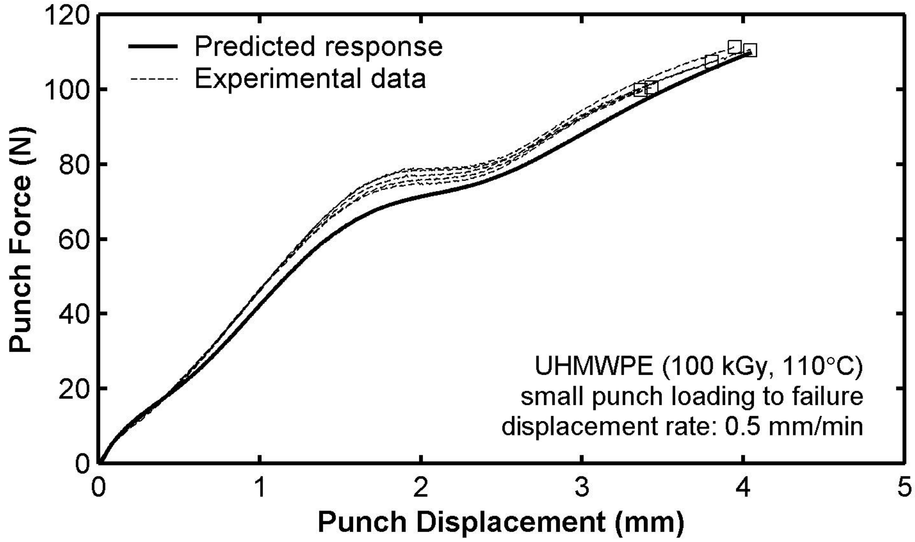

(b)

Figure 3. Comparison between the experimental data and Hybrid Model predictions: (a) uniaxial tension to failure, (b) small punch testing to failure. The experiments were performed on highly crosslinked UHMWPE annealed at 110°C. The failure points are indicated by the symbol □.

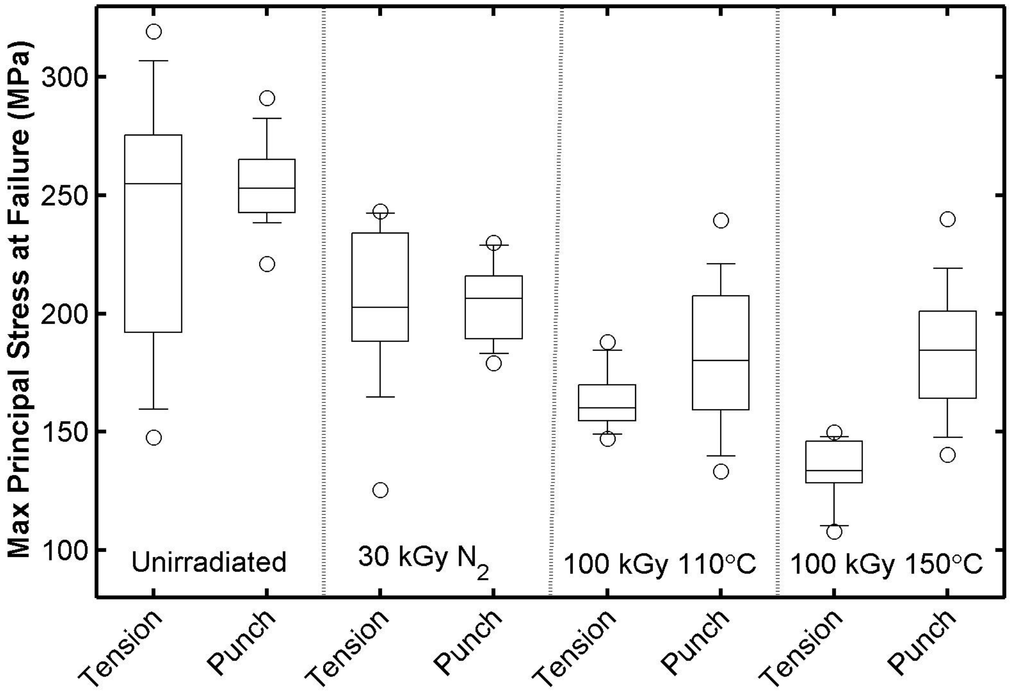
Max Principal Stress at Failure (MPa)
100
150
200
250
300
Unirradiated
30 kGy N$_2$
100 kGy 110°C
100 kGy 150°C
Tension
Punch
Tension
Punch
Tension
Punch
Tension
Punch

(a)

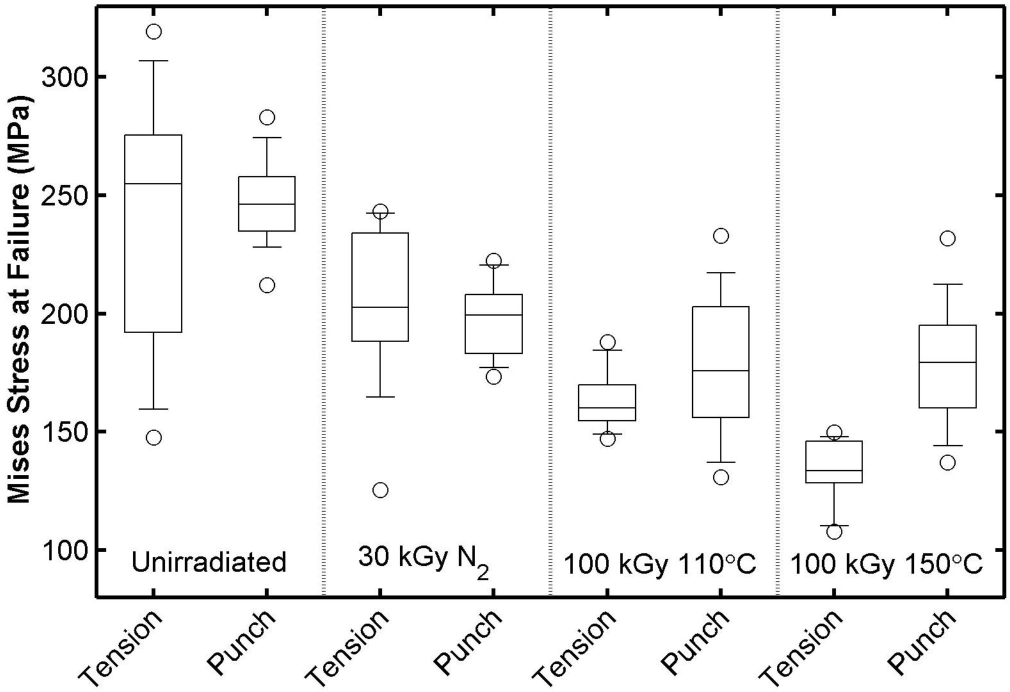
Mises Stress at Failure (MPa)
100
150
200
250
300
Unirradiated
30 kGy N$_2$
100 kGy 110°C
100 kGy 150°C
Tension
Punch
Tension
Punch
Tension
Punch
Tension
Punch

(b)

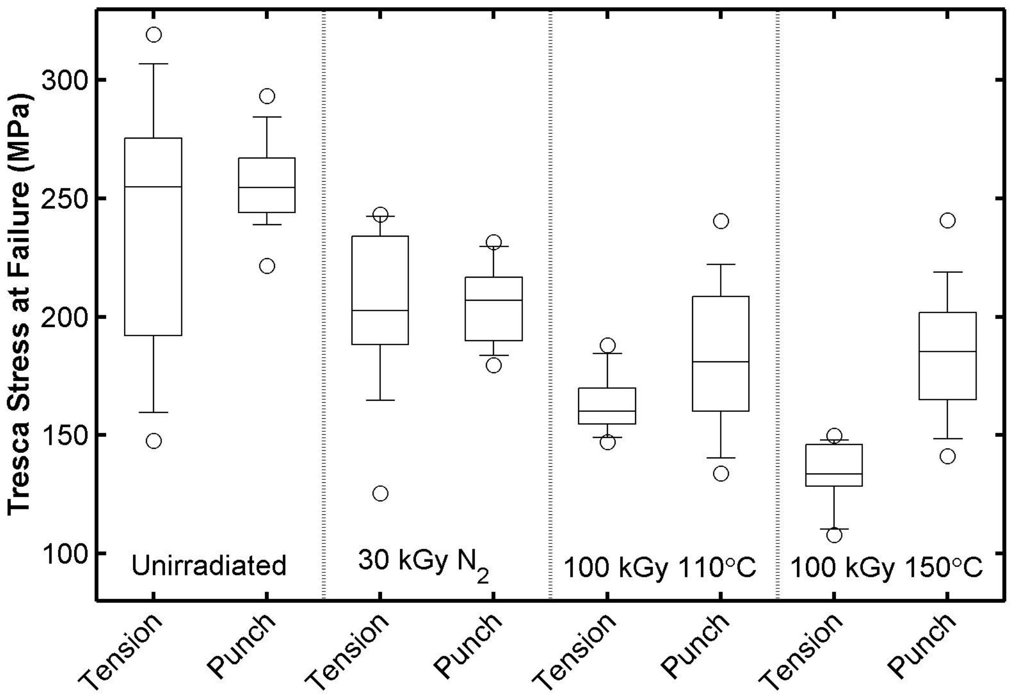

Tresca Stress at Failure (MPa)
100
150
200
250
300
Unirradiated
30 kGy N$_2$
100 kGy 110°C
100 kGy 150°C
Tension
Punch
Tension
Punch
Tension
Punch
Tension
Punch

(c)

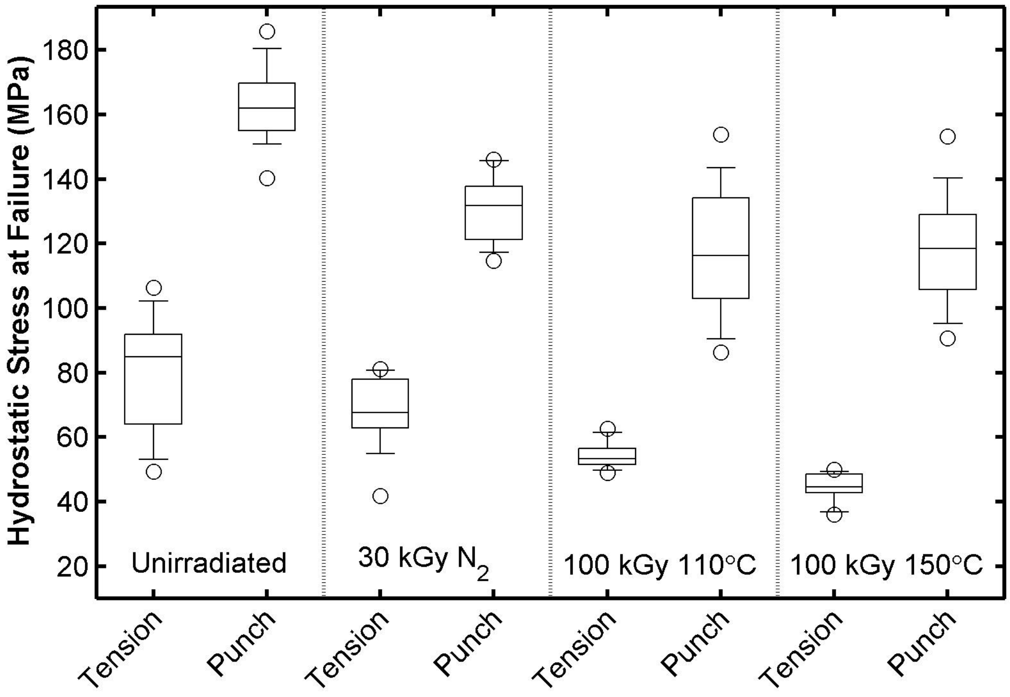

Hydrostatic Stress at Failure (MPa)
20
40
60
80
100
120
140
160
180
Unirradiated
30 kGy N$_2$
100 kGy 110°C
100 kGy 150°C
Tension
Punch
Tension
Punch
Tension
Punch
Tension
Punch

(d)

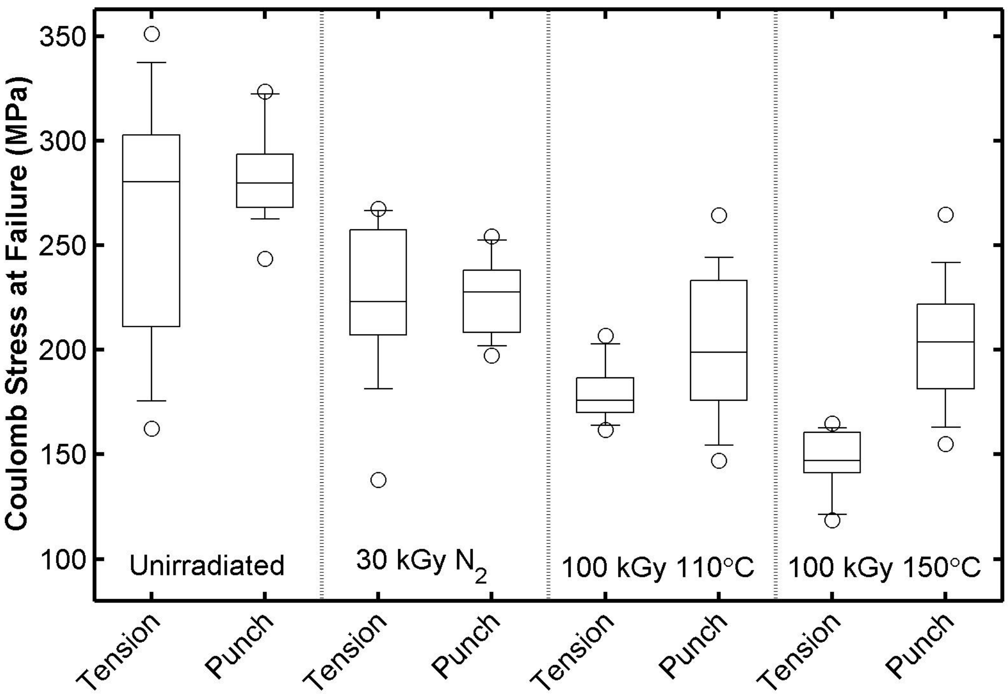

Coulomb Stress at Failure (MPa)
350
300
250
200
150
100
Unirradiated
30 kGy N_2
100 kGy 110°C
100 kGy 150°C
Tension
Punch
Tension
Punch
Tension
Punch
Tension
Punch

(e)

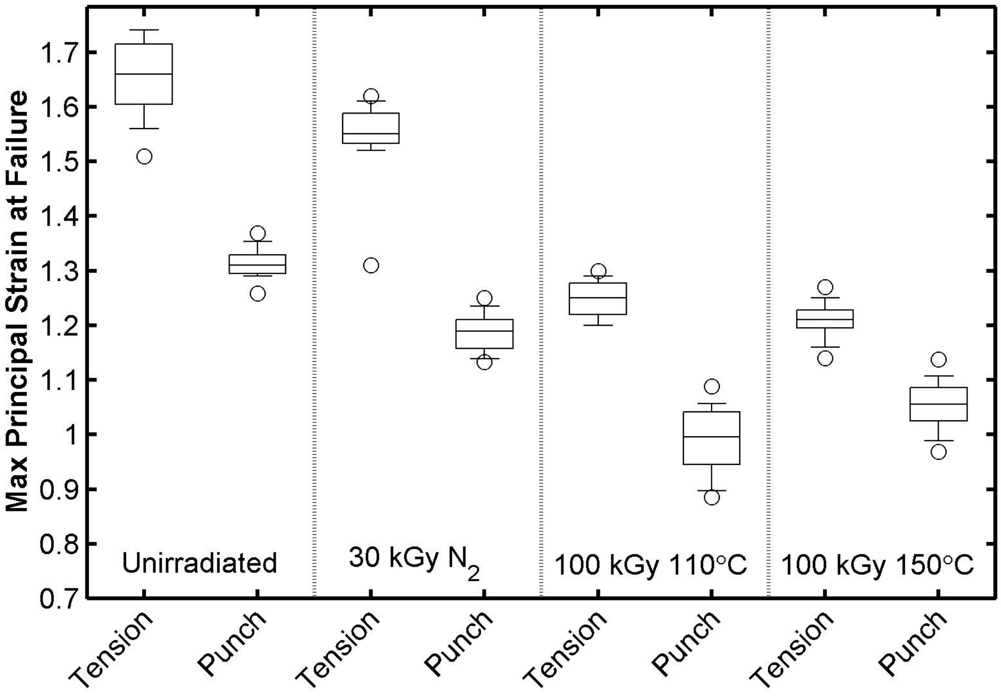

Max Principal Strain at Failure
1.7
1.6
1.5
1.4
1.3
1.2
1.1
1
0.9
0.8
0.7
Unirradiated
30 kGy N_2
100 kGy 110°C
100 kGy 150°C
Tension
Punch
Tension
Punch
Tension
Punch
Tension
Punch

(f)

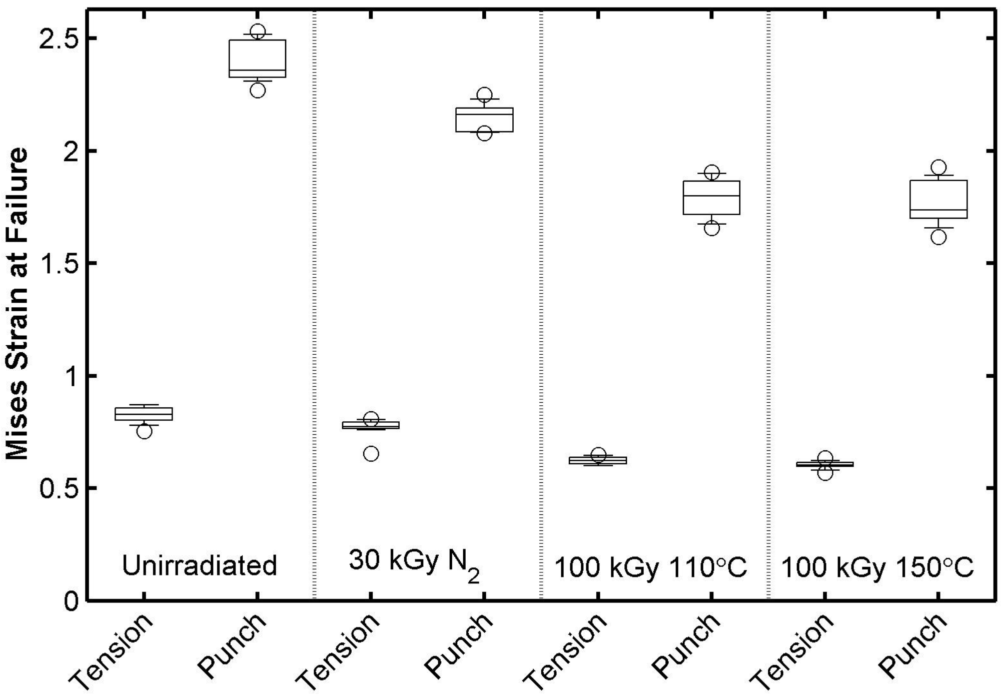
Mises Strain at Failure
0
0.5
1
1.5
2
2.5
Unirradiated
30 kGy N_2
100 kGy 110°C
100 kGy 150°C
Tension
Punch
Tension
Punch
Tension
Punch
Tension
Punch

(g)

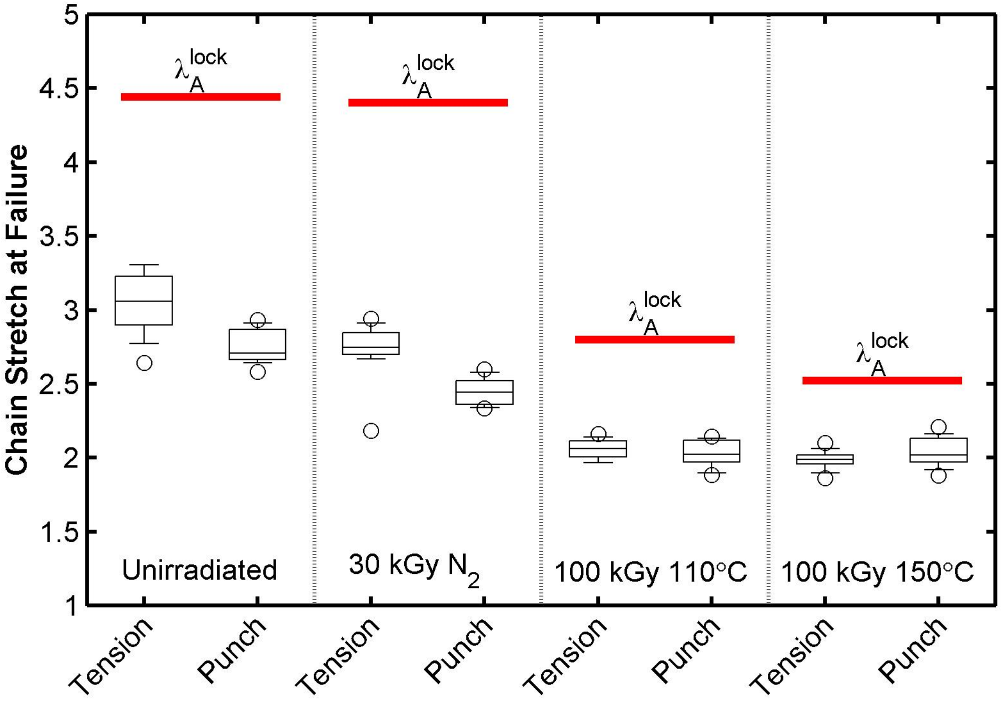
Chain Stretch at Failure
1
1.5
2
2.5
3
3.5
4
4.5
5
λ_A^{lock}
λ_A^{lock}
λ_A^{lock}
λ_A^{lock}
Unirradiated
30 kGy N_2
100 kGy 110°C
100 kGy 150°C
Tension
Punch
Tension
Punch
Tension
Punch
Tension
Punch

(h)

Figure 4. Predicted failure conditions in uniaxial tension and small punch loading of the four different types of UHMWPE examined: (a) maximum principal stress; (b) Mises stress; (c) Tresca stress; (d) hydrostatic stress; (e) Coulomb stress; (f) max principal strain; (g) Mises strain; (h) chain stretch.

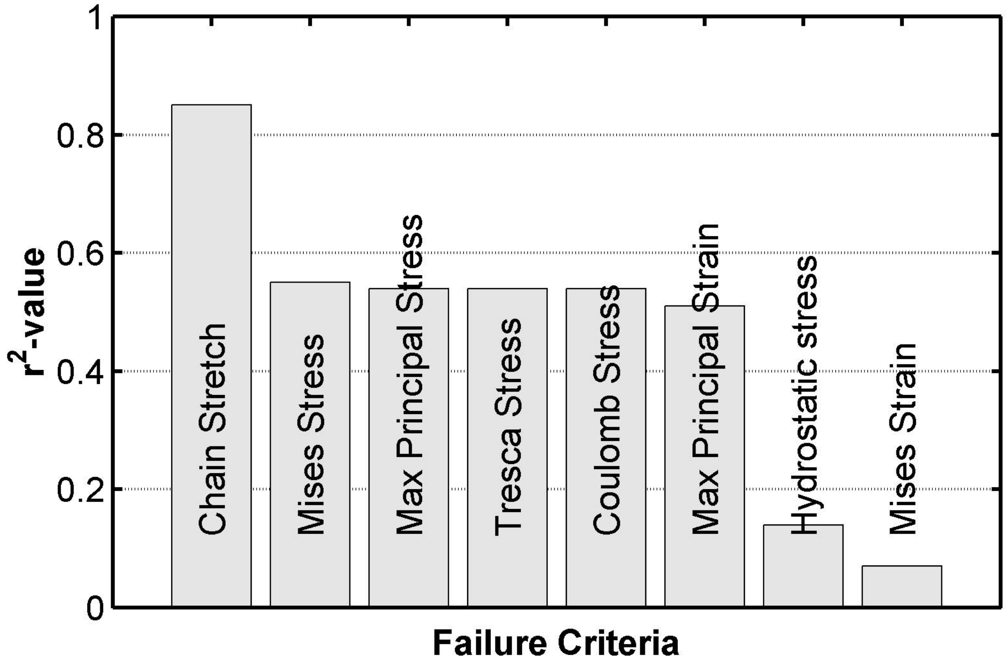

Figure 5. Average r^2-value for all four materials for the different failure models.

List of Tables

Table 1. Experimentally determined failure conditions for the nine failure models and the four materials. 33

Table 2. Comparison between the experimentally observed chain stretch at failure and the chain locking stretch parameter. 34

Table 3. Hybrid model material parameters for each of the four UHMWPE materials used in the tension and small punch simulations. 35

Table 1. Experimentally determined failure conditions for the eight failure models and the four types of UHMWPE.

Failure Condition	**Unirradiated**	**30 kGy (γ-N_2)**	**100 kGy (110°C)**	**100 kGy (150°C)**
Max principal stress (MPa)	246.2 (39.7)	204.1 (25.6)	172.1 (25.4)	158.2 (33.8)
Mises stress (MPa)	242.1 (39.1)	200.6 (25.6)	170.3 (24.4)	156.6 (31.3)
Tresca stress (MPa)	246.9 (39.9)	204.4 (25.7)	172.6 (25.6)	158.6 (34.0)
Hydrostatic stress (MPa)	120.8 (44.8)	99.2 (33.5)	85.9 (35.4)	81.1 (39.6)
Coulomb stress (MPa)	271.8 (44.3)	224.8 (28.2)	190.1 (28.6)	174.4 (37.4)
Max principal strain	1.48 (0.18)	1.37 (0.19)	1.12 (0.14)	1.13 (0.09)
Mises strain	1.61 (0.80)	1.46 (0.70)	1.12 (0.60)	1.19 (0.59)
Chain stretch	2.90 (0.22)	2.60 (0.21)	2.04 (0.08)	2.01 (0.08)

Table 2. Comparison between the experimentally observed chain stretch at failure and the chain locking stretch parameter.

	Unirradiated	**30 kGy (γ-N_2)**	**100 kGy (110°C)**	**100 kGy (150°C)**
Chain stretch at failure	2.90	2.60	2.04	2.01
Chain locking stretch parameter	4.44	4.40	2.80	2.52

Table 3. Hybrid model material parameters for each of the four UHMWPE materials used in the tension and small punch simulations.

Material Parameter	**Unirradiated**	**30 kGy γ-N$_2$**	**100 kGy 110°C**	**100 kGy 150°C**
E_e (MPa)	1574	2020	2009	1270
ν_e	0.46	0.46	0.46	0.46
μ_A (MPa)	7.73	8.22	10.15	8.14
λ_A^{lock}	4.44	4.40	2.80	2.52
κ_A (MPa)	2000	2000	2000	2000
q_A	0.20	0.20	0.20	0.20
s_{Bi}	40.0	40.0	40.0	40.0
s_{Bf}	10.0	10.0	10.0	10.0
p_B	27.0	27.0	27.0	27.0
τ_B^{base} (MPa)	26.1	25.0	26.2	20.7
m_B	9.5	9.5	9.5	9.5
τ_C^{base} (MPa)	8.0	8.0	8.5	8.5
m_C	3.3	3.3	3.3	3.3